AN OBJECT-BASED BURNT AREA DETECTION METHOD BASED ON LANDSAT IMAGES – A STEP FORWARD FOR AUTOMATIC GLOBAL HIGH-RESOLUTION MAPPING

E. Woźniak [a], S. Aleksandrowicz [a,*]

[a] Space Research Centre, Polish Academy of Sciences, Bartycka 18A, 00-716 Warsaw, Poland (ewozniak@cbk.waw.pl, saleksandrowicz@cbk.waw.pl*)

KEY WORDS: forest fires, automatic classification, HR mapping

ABSTRACT:

This study presents an algorithm for automatically mapping burnt areas using high-resolution images. It is applied to the Landsat 4, 5, 7 and 8 Land Surface Reflectance product; specifically, images acquired before and after (or during) the same fire season. It is also possible to extend the timeframe and use reference images acquired in the preceding year. This approach was adopted as cloudiness can make the acquisition of long time series impossible. A second advantage is that it avoids huge data transfers. The algorithm combines traditional, pixel-based image processing (calculation of spectral indexes and image differentiation) with object-based procedures (segmentation, reclassification, neighbourhood analysis) and consists of four steps. First, spectral indices (the Normalized Difference Vegetation Index and Normalised Burnt Ratio), and differences between image layers are calculated. The second is a multi-resolution segmentation, which uses the Normalised Burnt Ratio and near infrared layers. At this phase, masking of clouds, water and deserts takes place using atmospherically-corrected Landsat images. This is followed by the classification of 'core' burnt areas based on automatically-adjusted thresholds. The characteristics of the whole image (excluding clouds, deserts and water bodies) are analysed to develop functions that establish these thresholds. The fourth step consists of neighbourhood analysis. This focuses on objects that have not been classified as burnt areas, but whose spatial and spectral distances suggest that they may be part of them. The algorithm was tested in various areas (e.g. Spain, Greece, Siberia, California, Australia and Zambia). Comparisons with manual interpretation show that the fully-automated classification is very accurate (80–100%). The algorithm can be also applied to MODIS and Sentinel-2 data. It was developed within the framework of the Advanced Forest Fire Fighting (AF3) project, and the results have been used for damage and risk assessment.

1. INTRODUCTION

1.1 Literature overview

The reconstruction, understanding and characterization of the fire history of a terrain is important for improving fire management practices, risk prediction and damage assessment. It also extends our knowledge of the environmental and socioeconomic impacts of fire, climate change, the carbon cycle, biodiversity, ecosystem functioning, and interactions between land use and vegetation. Burnt area mapping defines at least three very important aspects of the fire regime: spatial pattern, size distribution and frequency.

Satellite remote sensing has proven to be an excellent source of information about forest fires. Burnt area studies have been carried out successfully all over the world: in tropical environments (Malingreau et al. 1985, Libonati et al. 2010), in savannas and grassland environments (Silva et al. 2005, Goodwin & Collett 2014, Hardtke et al. 2015), in Mediterranean zones (Fernandez et al. 1997, Garcia & Chuvieco 2004, Quintano et al. 2011), and in boreal forests (Laboda et al. 2007, Chen et al. 2016).

Several spectral indices and classification methods have been developed and tested to map burnt areas; these include the Normalised Difference Vegetation Index (NDVI) (Rouse et al. 1973, Chuvieco et al. 2002), the Global Environmental Monitoring Index (Pinty & Verstraete 1992), the Normalised Burnt Ratio (NBR; the normalised difference of Landsat TM Bands 4 and 7), multi-temporal variations (Key & Benson 1999, Miller & Thode 2007, Veraverbeke et al. 2001) and the Burnt Area Index (Martin 1998). Similarly, a wide range of methods are used for fire monitoring: manual digitalisation of burned areas (Silva et al. 2005), near-real-time active fire detection (Giglio et al. 2006), spectral indices (Martin et al. 2006, Laboda et al. 2007), image thresholding (Libonati et al. 2010, Maier 2010, Quintano et al. 2011), fire radiative power estimation (Maier et al. 2013, Williamson et al. 2013), time series analysis (Goodwin & Collett 2014, Hardtke et al. 2015), object-based approaches (Katagis et al. 2014), and Synthetic Aperture Radar and optical data fusion (Stroppiana et al. 2015).

1.2 Purpose of the study

Regional- and global-scale studies of burnt areas have been performed on low resolution (5 km) National Oceanic and Atmospheric Administration (NOAA) Advanced Very High Resolution Radiometer (AVHRR), or medium-resolution (1 km) Moderate Resolution Imaging Spectroradiometer (MODIS) data (Barbosa et al. 1999, Justice et al. 2002, Roy et al. 2005, Giglio et al. 2006). Historically, high costs and manual or semi-automated mapping methods have limited the use of Landsat images (30 m spatial resolution) to local studies (Russell-Smith et al. 1997, Edwards et al. 2001, Recondo et al. 2002, Felderhof & Gillieson 2006). However, the Landsat archive was made freely available in 2008, and surface reflectance data is available from 1984 to the present day. Similarly, Sentinel-2 data is freely available. On the other hand, limitations related to image classification methods remain, which highlights the need for the development of automatic classification algorithms for high-resolution data.

Changes in vegetation cover are often unrelated to fire, and can be caused by other factors such as phenological changes, harvesting or soil moisture. In addition, burnt areas are inhomogeneous and their spectral signature is closely related to fire intensity, fuel type, the meteorological conditions of

* Corresponding author

combustion, etc. These factors make the development of automated approaches difficult, and require balancing omission and commission errors (Goodwin & Collett 2014). Furthermore, it may not be possible to transfer methods to other locations or timeframes without recalibration.

Bastarrika et al. (2011) proposed an automated two-phase approach to mapping burnt areas (core burnt pixel identification and burnt region growth) using a series of single date Landsat TM/ETM+ imagery. The algorithm was calibrated and applied to Portugal and California (kappa coefficient = 0.85). A similar approach was applied in the Mediterranean region (Stroppiana et al. 2012), while a trend analysis formed the basis for automatic burnt area mapping in Australia (Goodwin et al. 2014).

Following these studies, this paper describes an algorithm for the automatic mapping of burnt areas. It combines a classical approach, based on the difference between pre- and post-fire images, with an object-based thresholding approach. Full automatization is the result of a recalibration procedure, specifically functions are developed for various parameters. that adjust thresholds between unburnt and burnt areas basing on the difference between pre- and post-fire images. As the method works on two images, it does not require long time series (unlike trajectory analysis methods). This is an important benefit given the burden of data transfer for global mapping, and cloud cover that can prevent the creation of long time series.

2. METHOD

2.1 Data

The algorithm uses atmospherically-corrected pairs of multispectral optical images (the Landsat 4, 5, 7, and 8 Surface Reflectance product). This product is supplied with cloud and water masks, which are also used. Acquisition dates are key to the algorithm's performance. The first (reference) image should be acquired before the fire season. The second image should be acquired during, or shortly after, it. Alternatively, a reference image acquired one year before the fire season image can be used with no loss of accuracy. Finally, the algorithm requires a thematic layer, namely, the slope layer calculated from Shuttle Radar Topography Mission elevation data.

The algorithm was tested on long time series for two regions in Greece: the surroundings of Athens (path 184 row 34) and the island of Cephalonia (path 185 row 33) and other scenes worldwide (California, Israel, central Siberia, northern and southern Spain, and Australia).

2.2 Proposed workflow

Figure 1 presents an overview of the method. It consists of four main steps: (1) the calculation of spectral indices and band differences; (2) the segmentation and exclusion of water bodies, desert and cloud; (3) the detection of 'core' burnt areas; and (4) region growing. All steps were implemented in eCognition software.

2.3 Raster arithmetic

The first step consists of calculating a set of additional layers based on pre- and post-fire scenes. The NBR (Key & Benson 2002) is calculated, along with the NDVI (Rouse at al. 1974).

$$\mathrm{NBR} = \frac{\mathrm{NIR\text{-}SWIR}}{\mathrm{NIR+SWIR}} \quad (1)$$

The differences in near infrared (NIR), short wave infrared (SWIR1, SWIR2) spectral bands and NBR for pre- and post-fire images are calculated. These differences are expressed as relative values and calculated as follows:

$$NBR_{DIFF} = 100 - \frac{NBR_{T2} * 100}{NBR_{T1}} \quad (2)$$

where $_{T1}$ is the pre-fire image, and $_{T2}$ is the post-fire image.

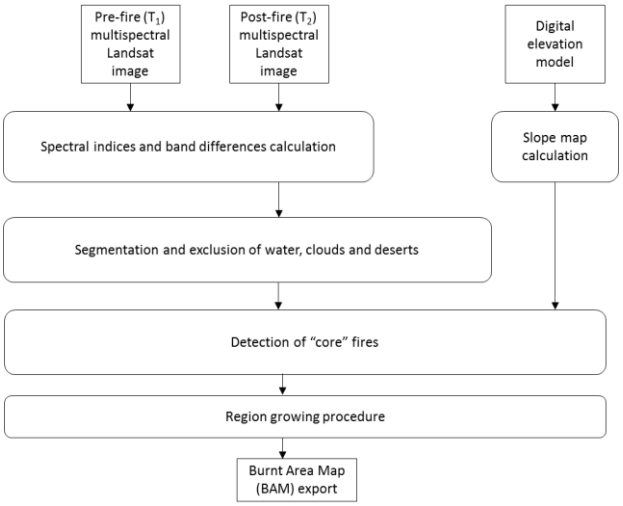

Figure 1. Burnt Area Mapping workflow

2.4 Segmentation

Segmentation starts with masking water, cloud and desert, which are excluded from further analysis. The aim is to reduce computation time and avoid any interference with the automatic thresholding process. The first step is based solely on Landsat thematic layers, and segments are classified into an 'exclude from analysis' group. For example, desert areas are masked based on a comparison of the NDVI index for the two images (which should be low in both cases). The second step concerns multiresolution segmentation. Segmentation layers NBR_{T1}, $NBR_{T2\text{-}T1}$, and $NIR_{T1\text{-}T2}$ are weighted. The scale parameter is fixed and remains unchanged when moving from one scene to another.

2.5 Core burnt areas classification

The classification of core burnt areas starts with a coarse classification of the NBR_{T2} layer (Figure 3a). Objects with a low NBR are considered as potential burnt areas. Specifically, objects with $\mu_o < (\mu_2 - \sigma_2)$ (where μ_o is the mean NBR, μ_2 is the mean NBR for the scene, and σ_2 is the standard deviation for the scene) are classified as *_temp*. In the next step, thresholds between unburnt and burnt areas are calculated as a function of the difference between pre- and post-fire images.

$$\mathrm{threshold} = \mathrm{f}(\mathrm{image}_{\mathrm{difference}}) \quad (3)$$

Threshold functions were obtained for all parameters from a reference dataset of pairs of images in different regions. The burnt areas were mapped manually using this dataset. Statistics for unburnt and burnt segments were extracted from the difference image for all parameters and used to calculate thresholds. Thresholds were calculated on the base of the normal distribution (Woźniak et al. 2016). The polynomial regressions between thresholds and difference image were found. An example of a thresholding function is given in Figure 2. Functions for $SWIR1_{DIFF}$, $SWIR2_{DIFF}$, G_{T2}, R_{T2} are established in the same way. Areas previously excluded from the analysis (clouds, water, desert) are not taken into account.

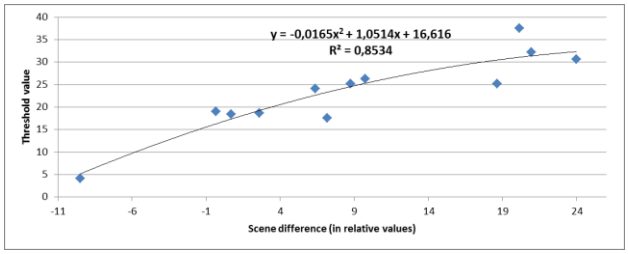

Figure 2. Relationship between scene difference and threshold for burnt and unburnt areas discrimination

However, although the results are good, the approach produces two types of misclassification. The first is the misclassification of crops that are harvested between data acquisitions as burnt areas. The second relates to partial omissions due to the inhomogeneous nature of burnt areas. The first problem is easily addressed using a slope map, as crop areas are usually found on plains Region growing provides a solution for the latter problem.

2.6 Region growing

Region growing (Figure 3c) starts with merging objects classified as core burnt areas. Neighbouring objects are classified based on their spectral distance from the core, calculated as the standard deviation of all areas classified as burnt in a scene. If a neighbouring object is classified as a burnt area it is merged into the core and the process is repeated.

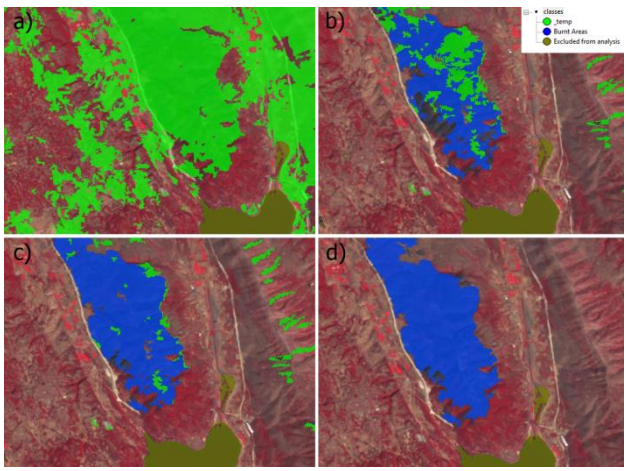

Figure 3. a) Initial NBR classification, b) classification of core burnt areas, c) region growing, d) post-processing

2.7 Post-processing

Post-processing is the final step of the classification (Figure 3d). Here, objects are merged and the minimum mapping unit (1ha) is applied. An enclosure analysis corrects burnt areas obscured by clouds.

3. RESULTS

The method was tested for all Landsat satellites in various geographical areas. For the island of Cephalonia and the surroundings of Athens all available Landsat scenes (for years in which at least two acquisitions were available) were classified. Robustness was tested on scenes from Siberia, northern and southern Spain, California, Israel and Australia. Burnt area mapping was validated using stratified random sampling. Stratification was based on the area of detected classes. One point indicated 100 pixels of burnt area and 1, 000 or 10, 000 pixels classified as unburnt depending on the percentage of the burnt area on the image scene. The results were compared with a manual classification of points. Mean overall accuracy for the tested scenes was 97.66% (mean kappa 0.86). Lowest values were obtained for scene from Athens from 1987 (respectively 85.79 and 0.25). Highest values were obtained also for scene from Athens from 1999 (respectively 99.94 and 0.95). Table 1 presents an example of a detailed confusion matrix for scene from Siberia.

		Classification			
		Burnt	Unburnt	Sum	
Reference	Burnt	14083	1069	15152	92,94
	Unburnt	1746	20892	22638	92,29
	Sum	15829	21961	34975	
		88,97	95,13	Overall accuracy	92,55

Table 1. Confusion matrix for scene from Siberia.

4. CONCLUSIONS

The burnt area mapping method presented here was tested in various areas (e.g. Spain, Greece, Siberia, California, Australia and Zambia). Threshold functions and the region growing procedure proved easily transferable, and accuracy remained satisfactory with no loss in automation.

The approach can also be applied to smaller-scale mapping. Following tuning of threshold functions and segmentation parameters, it was applied to MODIS Land Surface Reflectance (1000 m resolution) images. The results are more accurate than the fire estimates given in the MODIS QA layer.

Finally, similarities between Landsat and Sentinel-2 data mean that the algorithm can be fully automated when applied to the latter images, which offers an opportunity to fill in gaps in Landsat acquisitions.

ACKNOWLEDGEMENTS

The algorithm was developed within the framework of the Advanced Forest Fire Fighting (AF3) project (FP7-SEC-2013-1, grant agreement N°607276)

REFERENCES

Barbosa, P.M., Gregoire, J.M., & Cardoso Pereira, J.M. 1999. An Algorithm for Extracting Burned Areas from Time Series of AVHRR GAC Data Applied at a Continental Scale. *Remote Sensing of Environment*, 69(3), 253–263.

Bastarrika, A., Chuvieco, E., & Martín, M. P. 2011. Mapping burned areas from Landsat TM/ETM+ data with a two-phase algorithm: Balancing omission and commission errors. *Remote Sensing of Environment*, 115(4), 1003–1012.

Chen, W., Moriya, K., Sakai, T., Koyama L., & Cao, C.X. 2016. Mapping a burned forest area from Landsat TM data by multiple methods. *Geomatics, Natural Hazards and Risk*, 7(1), 384–402.

Chuvieco, E., Martín, M. P., & Palacios, A. 2002. Assessment of different spectral indices in the red-near-infrared spectral

domain for burned land discrimination. *International Journal of Remote Sensing*, 23, 5103−5110.

Edwards, A.C., Hauser, P., Anderson, M., McCartney, J., Armstrong, M., Thackway, R., et al. 2001. A tale of two parks: Contemporary fire regimes of Litchfield and Nitmiluk National Parks, monsoonal northern Australia. *International Journal of Wildland Fire*, 10, 79–89.

Felderhof, L., & Gillieson, D. 2006. Comparison of fire patterns and fire frequency in two tropical savanna bioregions. *Austral Ecology*, 31, 736–746.

Fernandez, A., Illera, P., & Casanova, J.L. 1997. Automatic mapping of surfaces affected by forest fires in Spain using AVHRR NDVI composite image data. *Remote Sensing of Environment* 60, 153–162.

Garcia, M., & Chuvieco, E. 2004. Assessment of the potential of SAC-C/MMRS imagery for mapping burned areas in Spain. *Remote Sensing of Environment*, 92, 414–423.

Giglio, L., van der Werf, G., Randerson, J., Collatz, G., & Kasibhatla, P. 2006. Global estimation of burned area using MODIS active fire observations. *Atmospheric Chemistry and Physics*, 6, 957–974.

Goodwin N.R., & Collett, L.J. 2014. Development of an automated method for mapping fire history captured in Landsat TM and ETM+ time series across Queensland, Australia. *Remote Sensing of Environment*, 148, 206–221

Hardtkea,L.A., Blancoa, P.D., del Vallea, H.F., Metternichtb, G.I., & Sionec, W.F. 2015. Semi-automated mapping of burned areas in semi-arid ecosystems using MODIS time-series imagery. *International Journal of Applied Earth Observation and Geoinformation*, 38, 25–35.

Justice, C. O., Giglio, L., Korontzi, S., Owens, J., Morisette, J. T., Roy, D., et al. 2002. The MODIS fire products. *Remote Sensing of Environment*, 83, 244–262.

Katagis, T., Gitas, I.Z., & Mitri, G.H. 2014. An Object-Based Approach for Fire History Reconstruction by Using Three Generations of Landsat Sensors. *Remote Sensing*, 6(6), 5480–5496

Key, C. H., & Benson, N. C. 1999. Measuring and remote sensing of burn severity. In L. F. Neuenschwander, & K. C. Ryan (Eds.), *Proceedings. Joint Fire Science Conference and Workshop*, Vol. II, Boise, ID, 15–17 June 1999: University of Idaho and International Association of Wildland Fire (284 pp.).

Loboda, T., O'Neal, & K., Csiszar, I. 2007. Regionally adaptable dNBR-based algorithm for burned area mapping from MODIS data. *Remote Sensing of Environment*, 109, 429–442.

Libonati, R., DaCamara, C., Pereira, J., & Peres, L. 2010. Retrieving middle-infrared reflectance for burned area mapping in tropical environments using MODIS. *Remote Sensing Environment*, 114, 831–843.

Maier, S. 2010. Changes in surface reflectance from wildfires on the Australian continent measured by MODIS. *International Journal of Remote Sensing*, 31, 3161–3176.

Maier, S., Russell-Smith, J., Edwards, A., & Yates, C. 2013. Sensitivity of the MODIS fire detection algorithm (MOD14) in the savanna region of the Northern Territory, Australia. *ISPRS Journal of Photogrammetry and Remote Sensing*, 76, 11–16.

Martín, M. P. 1998. *Cartografía e inventario de incendios forestales en la Península Ibérica a partir de imágenes NOAA–AVHRR*. Departamento de Geografía. Alcalá de Henares: Universidad de Alcalá.

Martín, M., Gómez, I., & Chuvieco, E. 2006. Burnt area index (BAIM) for burned area discrimination at regional scale using MODIS data. *For. Ecol. Manage*. 234s, s221.

Malingreau, J. P., Stephens, G., & Fellows, L. 1985. Remote sensing of forest fires: Kalimantan and North Borneo in 1982-83. *Ambio*, 14, 314–321.

Miller, J.D., & Thode, A. E. 2007. Quantifying burn severity in a heterogeneous landscape with a relative version of the delta Normalized Burn Ratio (dNBR). *Remote Sensing of Environment*, 109 (1), 66–80.

Pinty, B., & Verstraete, M. M. 1992. GEMI: a non-linear index to monitor global vegetation from satellites. *Vegetatio*, 101, 15−20.

Quintano, C., Fernández-Manso, A., Stein, A., & Bijker, W. 2011. Estimation of area burned by forest fires in Mediterranean countries: a remote sensing data mining perspective. *For. Ecol. Manage*, 262, 1597–1607.

Recondo, C., Woźniak, E., & Perez-Morandaira, C. 2002. Cartografia de zonas quemadas en Asturias durante el periodo 1991-2001 a partir de imaenes Landsat TM, *Revista de Teledeteccion*, 18, 47–55.

Rouse, J.W., Haas, R.H., Schell, J.A. & Deering, D.W. 1973. Monitoring vegetation systems in the great plains with ERTS. In, 3rd ERTS Symposium, 309–317 (NASA)

Roy, D., Jin, Y., Lewis, P., & Justice, C. 2005. Prototyping a global algorithm for systematic fire-affected area mapping using MODIS time series data. *Remote Sensing of Environment*, 97, 137–162.

Russell-Smith, J., Ryan, P. G., & Durieu, R. 1997. A Landsat MSS-derived fire history of Kakadu National Park. *Journal of Applied Ecology*, 34, 748–766.

Silva, J., Sá, A., & Pereira, J. 2005. Comparison of burned area estimates derived from SPOT-VEGETATION and Landsat ETM+ data in Africa: influence of spatial pattern and vegetation type. *Remote Sensing of Environment*, 96, 188–201.

Stroppiana, D., Bordogna, G., Carrara, P., Boschetti, M., Boschetti, L., & Brivio, P. A. 2012. A method for extracting burned areas from Landsat TM/ETM+ images by soft aggregation of multiple spectral indices and a region growing algorithm. *ISPRS Journal of Photogrammetry and Remote Sensing*, 69, 88–102.

Stroppiana, D., Azar, R., Calò, F., Pepe, A., Imperatore, P., Boschetti, M., Silva, J.M.N., Brivio, P.A., & Lanari, R. 2015. Integration of Optical and SAR Data for Burned Area Mapping in Mediterranean Regions. *Remote Sensing*, 7, 1320–1345

Veraverbeke, S., Lhermitte, S., Verstraeten, W.W., & Goossens, R. 2001. A time-integrated MODIS burn severity assessment using the multi-temporal differenced normalized burn ratio

(dNBRMT). *International Journal of Applied Earth Observation and Geoinformation*, 13, 52–58.

Williamson, G., Price, O., Henderson, S., & Bowman, D. 2013. Satellite-based comparison of fire intensity and smoke plumes from prescribed fires and wildfires in south-eastern Australia. *International Journal of Wildland Fire*, 22, 121–129.

Woźniak, E., Kofman, W., Wajer, P., Lewiński, S., & Nowakowski, A. 2016. The influence of filtration and decomposition window size on the threshold value and accuracy of land-cover classification of polarimetric SAR images. *International Journal of Remote Sensing*, 37(1), 212–228.